PAPER • **OPEN ACCESS**

Alloying effect of Ti-6Al-4V on composite of 321 stainless steel fabricated by electron beam additive manufacturing

To cite this article: K S Osipovich *et al* 2019 *IOP Conf. Ser.: Mater. Sci. Eng.* **537** 022075

IOP Conf. Series: Materials Science and Engineering **537** (2019) 022075 doi:10.1088/1757-899X/537/2/022075

Alloying effect of Ti-6Al-4V on composite of 321 stainless steel fabricated by electron beam additive manufacturing

K S Osipovich, K N Kalashnikov and A V Vorontsov

Institute of Strength Physics and Materials Sciences, SB RAS, 2/4 Akademicheskii Ave., Tomsk, 634055, Russian Federation

E-mail: osipovich_k@ispms.ru

Abstract. For the present significant progress has been made in understanding additive manufacturing processes Additive manufacturing techniques such as selective laser melting and laser-based directed energy deposition are widely used, but in comparison, electron-beam melting offers two unique advantages that are particularly important for titanium alloys: a high-vacuum medium and a preheating capacity for both substrate and feed material. This work describes experimental studies of a component built from 321 stainless steel and Ti-6Al-4V. The coating was formed through deposition of a wire with the use of a high-voltage electron beam in the high-vacuum medium. Two materials of deposition on the substrate were carried out in this study. As a result, 321 stainless steel composite coating can successfully form surface with gradient microstructure during EBAM cladding process. At Ti-6Al-4V of compositions was cracked, which led to the destruction of the top of the sample. The presence the intermetallic compounds of the top of the sample adversely affected of the composite that cracking occurred in the material.

1. Introduction

The modern world has a very high rate of development of technology. The main objective of development is to improve technological processes in order to improve the quality of technical devices and create new types of devices. Extreme-environment applications require parts that, for instance, must perform at radically different temperatures at different locations in the part [1]. Joining of dissimilar materials or functional grading of two or more materials is therefore required [2]. These materials can offer unique solutions to engineering problems. This approach has been previously tested to additively create various polymaterial structures, ranging from Ti [3], CoCrMo [4], stainless steel [5] and Inconel-based composites [6]. Additively manufactured materials have demonstrated improvements in properties such as hardness, wear resistance [7], and even reduction in elastic modulus [8] compared to single metal/alloy parts.

The research has been carried out in these sectors in developing various welding technique to produce high strength and low weight components. The thermal welding of Ti/Al dissimilar alloys is a challenge because of great dissimilarities in physical-chemical properties between Ti and Al [9]. Recently, surface modification with concentrated heating source, such as laser or electron beam radiation at reactive atmosphere (such as N) has been presented for titanium alloys. Although, the electron and laser beam surface processing time is very short, requiring vacuum chamber, costly manufacturing procedure and expensive initial investments are the main limitations of these processes [10].

Additive manufacturing (AM) is ideal for the constructive method of preparation of metallic structures. In particular, Electron Beam Melting, which uses electronic emitters, so-called electronic guns, as energy sources for melting in the high-vacuum medium.

In this paper the creation of metallic structures made of 321 stainless steel and Ti-6Al-4V in the process of electron-beam additive technology is investigated. Influence of printing parameters on macrostructure, formation of defects on the surface of polymetallic structures.

2. Materials and methods

The samples under study were obtained using the Laboratory Experimental Installation for additive electron-beam production of metal wire products as shown in figure 1. The device reads data from a file containing a three-dimensional digital model and applies sequential layers of material wire. The contours of the model layers are drawn by an electron beam that melts the wire at the point of contact. Melting is performed in vacuum working chambers, which allows working with materials sensitive to oxidation. Eight layers were deposited. Layers were approximately 1 mm tall [11].

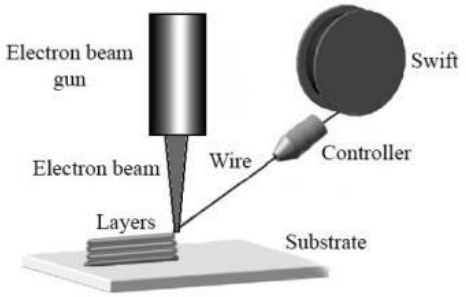

Figure 1. Schematic drawing of electron beam additive manufacturing.

321 stainless steel and Ti-6Al-4V wires of compositions noted in Table 1 were used. For optical metallography, samples were cut using electro-discharge machining and were mechanically ground and then polished and pickled in HOOC-COOH solution.

Table 1. Chemical composition of 321 stainless steel and Ti-6Al-4V wires used for electron beam melting.

	Ti	Fe	Cr	Ni	Al	V	Mn	Cu	Zr	Si	O	C	Other
321	-	~ 67	17-19	8-9.5	-	-	to 2	to 0.3	-	to 0.8	-	to 0.12	to 0.06
Ti-6Al-4V	86.4-91.2	to 0.3	-	-	5.3-6.8	3.5-5.3	-	-	to 0.3	to 0.15	to 0.2	to 0.1	to 0.07

For micro and macrostructure of the sample surface an Altami MET-1C microscope was used. The hardness distribution of the cross-section along the Z-axis direction was investigated using the micro Vickers hardness tester Duramin 5. The Vickers hardness test was conducted more than three times for each test point and the average value was plotted in the graph. Microhardness values are an average of five measurements, with standard deviation indicated by error line mark on the graph. The compartition of Fe and Ni in the cross section of the profile was investigated by scanning electron microscope SEMTRACK mini.

3. Results and discussions

Figure 2 (a) shows a crosscut of the built object. The samples were etched chemical action to visual the border between the materials. From the side view, the building up of the layers can be readily observed. Figure 2 (b) schematically shows the geometrical features for a single clad. In brief, a single clad has a

height, h (mm), which is the measure of its thickness above the adjacent substrate surface, has a width that is shown by w (mm), and has a penetration depth, b (mm), which is defined as the thickness of the substrate melted during cladding process and is just under the clad and below the substrate surface.

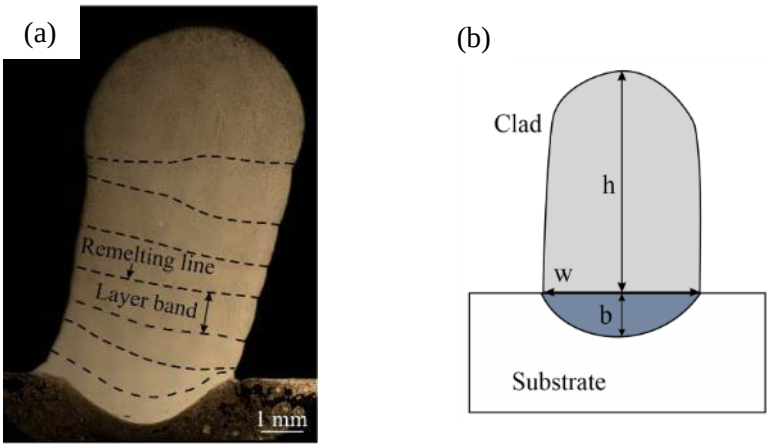

Figure 2. Macrostructure (a) and schematic design (b) of the sample of 321 stainless steel fabricated by electron beam additive manufacturing.

Analysis of the built object shows that various defects such as porosity and/or crack formation were not indicated, indicating a fully dense as deposited part. Hence the wettability between substrate and the buildup of the clad were good. The overall shape of the substrate was conserved, but had a deflected position. The limited mixing that occurred between the clad and the substrate was confined to less than 1.42 mm, as indicated by the interfacial region. This occurrence of local interaction may be related to the differences in respective fusion temperature T_{clad}^{321} = 1425 º C and T_{sub}^{fus} = 1500 º C.

Figure 3 (a) and (b) displays the morphology of the border between the materials. The cross section of clad is composed of substrate, bonding zone and clad. There exists a narrow bright strip at the bonding zone, which is the solution interface layer generated by the alloy interdiffusion between clad and substrate under the action of heat source. The microstructure of solution interface layer is planar grain zone with the width a few tens of microns. Over bright strip, there exists a zone without distinct microstructure, which is created when the planar grains grow epitaxially and slowly into the clad inner. Further, up on this figure 3, the dendrites appear and grow in the direction nearly vertical to the interface [12]. According to the related solidification theory proposed by Hunt [13], the ratio of temperature gradient G and solidification velocity VS, namely G/VS, is an important control parameter for the morphology preference of solidification microstructure. If G/VS is considerably great or VS tends to zero, then forming the planar grains. If G/VS is relatively great, then volume fraction of equiaxed grains is minor. Therefore, the solidification microstructure is prone to generate columnar dendrites. However, if G/VS is relatively small, then volume fraction of equiaxed grains is major.

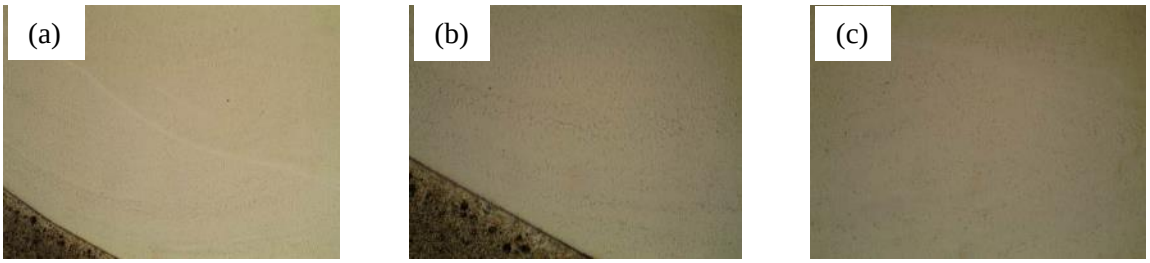

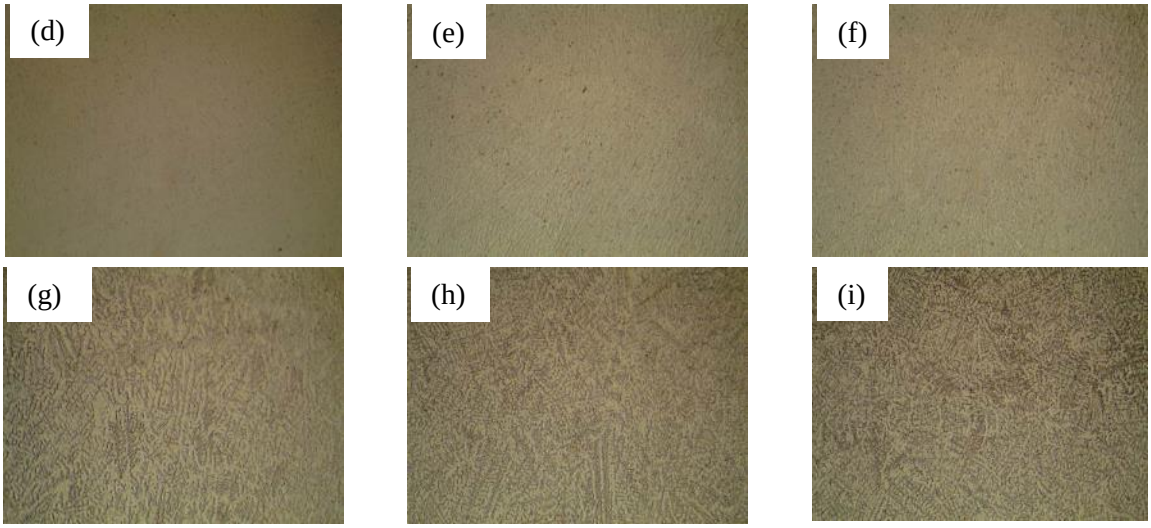

Figure 3. The optics microscopy of different areas of the substrate to the top of the sample.

In this experiment, G/VS is relatively great at the interface substrate and the build-up of the clad, accordingly the microstructure grows slowly with planar interface, thus forming the bright band composed of solid solution phase and the structural region without distinct microstructure characterization [13].

The microstructure is highly variable depending on the layers. Several areas are clearly visible even by the naked eye for their different etched degree. Microscopic observation of these areas by optical microscopy shows that morphologies of microstructure are quite different in these areas, as is shown in figure 3. The vermicular morphology of the delta ferrite is dominant at low layers, the structure having dendritic features (figure 3 (b)).

During the deposition process, a later deposition layer melted the upper part of the previous layer, which causes recrystallization. Fine and regular shape austenite grains were formed as a result of this recrystallization. Most of the austenite grains exhibited cellular (figure 3 (c)). The resulting gray-etching, blocky ferrite and the lacy, dark-etching networks in figure 3 (c) and (d) represent these primary dendrite cores. nucleates at the grain boundaries, occurs along specific habit planes in the ferrite; this ultimately results in the formation of alternate austenite and ferrite laths. With build-up of the layers the solidification microstructure changed from planar crystals into cellular dendrites and columnar dendrites along the direction toward the centre of the deposition, as shown in figure 3 (e – f). Different grain morphologies were found for the dendritic and cellular crystals with different growth directions, especially in the middle part of the deposition sample (figure 3 (g – i). Microstructural examination of the built specimen that a zone of gradient was successfully produced.

The microstructure obtained at Ti of compositions is given in figure 4. As can be seen from the composite, Ti decomposed and the material was cracked, which led to the destruction of the top of the sample. There are tunnel shaped defects apparent, cavity, crack and microcrack in resulting from insufficient consolidation. During fabrication metallic parts experience a complex thermal history involving directional heat extraction, and repeated melting and rapid solidification.

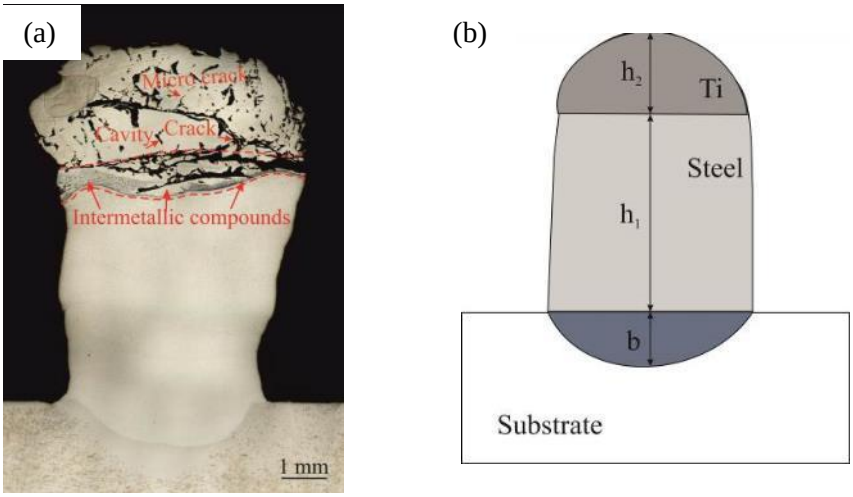

Figure 4. Macrostructure (a) and schematic design (b) of the sample of 321 stainless steel and Ti-6Al-4V fabricated by electron beam additive manufacturing.

The structure samples of top had a transition of composition variation across the layer (figure 5). The horizontal axis shows the distance from the bottom to the top of sample. Composition analysis from the substrate toward top of sample shows that the Fe content falls significantly to 46.856 ± 2.490 wt. % and the Ti content rises significantly sharply to 30.189 ± 1.536 wt. % in the area from 5.5 mm to 6.5 mm away from the substrate. Then the Fe content decrease smooth to 36.613 ± 2.413 wt. % whilst Ti content increases to 40.254 ± 1.920 wt. % to a constant level.

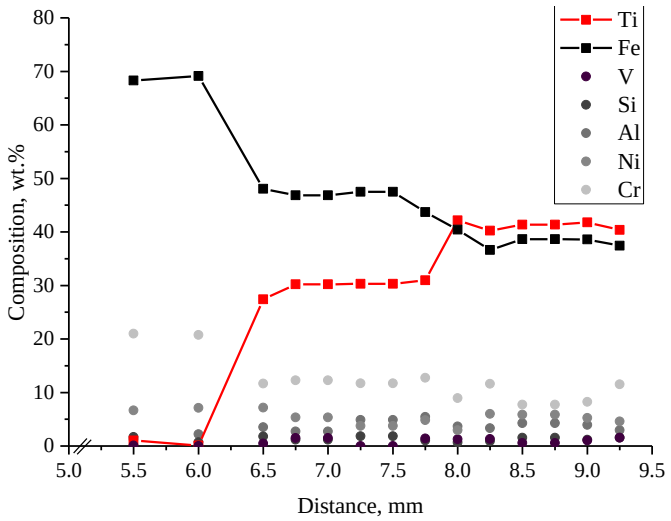

Figure 5. Measured composition of the sample of 321 stainless steel and Ti-6Al-4V fabricated by electron beam additive manufacturing.

As shown in figure 5, the amounts of Fe and Ti near the inter-face between 321 stainless steel and Ti-6Al-4V change greatly. The amounts of Fe and Ti were constant in other areas. The amount of Ti changed in the area from 7.75 mm to 8.00 mm away from the bottom of the test piece. The Fe distribution had the same tendency. A range where the smooth amount of Fe changed was about 0.75 mm. The precipitate intermetallic compounds in this area give rise crack. Table 2 shows the elemental analysis results of the top of the sample from figure 6 (a – c).

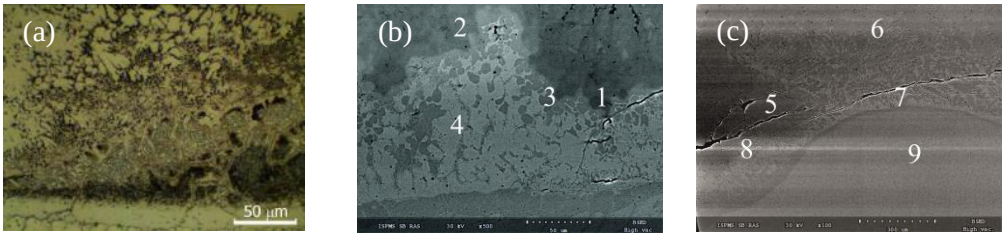

Figure 6. The micrograph of the interface between 321stainless steel and Ti-6Al-4V.

Intermetallic compounds of elemental composition noted in Table 2.

Table 2. Intermetallic compounds of elemental composition.

Elt.	Area	Al	Si	Ti	V	Cr	Fe	Ni
Conc, wt. %	**1**	3.144	1.315	20.217	0.000	13.065	53.056	9.203
	2	3.918	1.237	46.907	1.517	6.297	33.269	6.856
	3	4.198	1.175	51.529	1.090	5.721	30.959	5.328
	4	2.064	1.272	14.561	0.117	18.474	56.767	6.746
	5	1.170	1.166	22.403	0.087	12.645	54.384	8.144
	6	1.999	1.247	28.798	0.646	9.896	51.670	5.745
	7	1.337	1.202	0.148	0.157	19.122	70.999	7.035
	8	3.107	1.028	3.126	0.066	19.485	65.999	7.189
	10	2.819	1.905	0.643	0.218	19.764	63.590	11.062

As can be seen, the gray zone is rich in Ti (46.907 wt. % compared to 51.527 wt. %) and is depleted in Fe (30.959 wt. % compared to 33.269 wt. %); in comparison, the dark zone shows less content in Ti (20.217 wt. % to 28.798 wt. %) and above content of Fe (51.670 wt. % to 54.384 wt. %); the light zone shows deficiency of Ti and rich in Fe (63.590 wt. % to 70.999 wt. %). Such a Ti depleted zone could occur due to the enhanced elemental segregation during the deposition process.

For further identification of phase structures, an X-ray structural analysis was performed (figure 7 (a)).

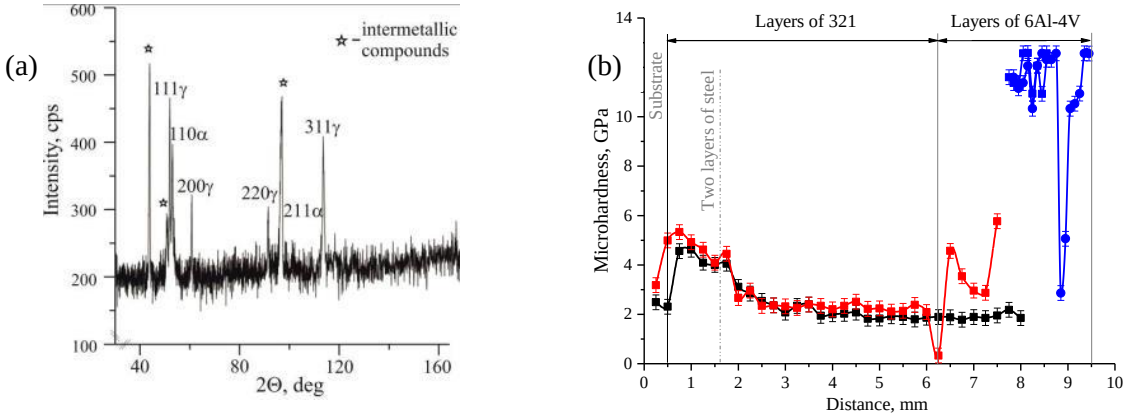

Figure 7. X-ray diffraction patterns (a) and microhardness (b) of the sample of 321 stainless steel and Ti-6Al-4V fabricated by electron beam additive manufacturing.

According to the results of X-ray phase analysis, it can be seen that the sample is comprised of the γ- and α-Fe. In the contact zone of dissimilar layers is represented by two phases of a solid solution and several intermetallic phases consisting of Fe compounds with Ni.

Thus, the intermetallic compounds consisting of Fe compounds with Ni would strengthen the material compared. In addition, the consolidation of 321 stainless steel and Ti-6Al-4V compounds reduced the overall strength. The hardness distribution of the cross-section shown in figure 7 (b).

The red line shown in figure 8 indicates the hardness of Ti compounds. The hardness trends shift at the interfaces and then smooth out as a function of distance away from the interface. The hardness of the material two layers of 321 stainless steel deposited on substrate is equal to 5.3 GPa that is considerably higher in comparison with the value of 3 GPa determined in the base area. These increases in hardness were due to exists a zone without distinct microstructure as small as 0.5 mm. In the direct deposit structure of 321 stainless steel in both samples the hardness values between 1.6 mm and 6.0 mm is equal 2.36 ± 0.29 GPa. The hardness of Ti-6Al-4V layer deposited on a 321 steel layers jumped from 4.57 GPa to 5.77 GPa. Hardness on the side layers of 321 steel remains nearly constant. The graph shows that the hardness of the Ti-6Al-4V is significantly higher than that of layers of 321 steel. The hardness trend in the top of sample, however, does precisely overlie the center of sample. Because were achieved high values of hardness within the top deposited layer. They average around 11.68 ± 0.29 GPa. Higher hardness values could also be attributed to intermetallic compounds, as shown in figure 7 (b).

4. Results and discussions

Metallic structures of 321 stainless steel and Ti-6Al-4V have been successfully processed using electron beam additive manufacturing. However, the composite with buildup of the Ti-6Al-4V was decomposed. It is found that proceeding from 321 stainless steel to Ti-6Al-4V characteristically of the Fe content decrease smooth to 36.613 ± 2.413 wt. % whilst Ti content increases to 40.254 ± 1.920 wt. % along the height of the buildup deposit. The presence the intermetallic compounds of the top of the sample adversely affected of the composite that cracking occurred in the material. Tunnel shaped defects apparent, cavity, crack and microcrack was recognized. But the intermetallic compounds strengthen of the Vickers hardness within the top deposited layer to around 11.68 ± 0.29 GPa.

Acknowledgments

This work was performed within the frame of the Fundamental Research Program of the State Academies of Sciences for 2013-2020, line of research III.23.

References

[1] Shakil M, Ahmad M, Tariq N H *et al* 2014 *Vacuum* **110** pp 121-6
[2] Lima D D, Mantri S A, Mikler C V *et al* 2017 *Mater. Des*. **130** pp 8–15
[3] Sahasrabudhe H, Bose S and Bandyopadhyay A 2018 *Acta Biomater*. **66** pp 118–28
[4] Sahasrabudhe H, Harrison R, Carpenter C and Bandyopadhyay A 2015 *Addit. Manuf.* **5** pp 1–8
[5] Gualtieri T and Bandyopadhyay A 2018 *Mater. Des.* **139** pp 419–28
[6] Das M, Bhattacharya K., Dittrick S A *et al* 2014 *J. Mech. Behav. Biomed. Mater*. **29** 259–71
[7] Mahamood R M and Akinlabi E T 2017 (*Springer International Publishing, Cham*) p 103
[8] Vaidya A W V, Horstmann M, Ventzke V, Petrovski B, Kocak M, Kocik R and Tempus G 2010 *J. Mater. Sci.* **45** 6242-54
[9] Sadeghimeresht E, Karimi P, Zhang P, Peng R *et al* 2018 Isothermal Oxidation Behavior of EBM-Additive Manufactured Alloy **718** 1–22
[10] Ghosh S, Ma L, Ofori-Opoku N and Guyer J E 2017 *Model. Simul. Mater. Sci. Eng*. **25 (6)** 065002
[11] Kalashnikova T A, Khoroshko E S, Chumaevskii A V and Filippov A V 2018 *AIP Conference Proceedings* **2051** 020114
[12] Gnyusov S F and Tarasov S Y 2013 *Surface and Coatings Technology* **232** pp 775-83
[13] Zhang K, Wang S, Liu W and Shang X 2014 *Materials & Design* **55** pp 104-19